Proc. of SPIE Vol. 0450, Structural Mechanics of Optical Systems I, ed. L.M. Cohen (Jan 1983) Copyright SPIE

Thermal Distortion of a Thin Low Expansion Fused Silica Mirror

John W. Pepi
and
William P. Barnes, Jr.

Itek Optical Systems
A Division of Litton Industries
10 Maguire Road
Lexington, MA 02173

To meet the demands of a fraction of a wavelength of light residual error imposed by high resolution optical systems, detailed analytical modeling techniques are required. For large lightweight, optical elements, errors can be significant even in a relatively benign thermal environment with materials exhibiting near zero coefficient of thermal expansion (CTE). This study evaluates a thin, circular, spherical mirror made of Corning Glass Works Ultra Low Expansion (ULE) fused silica glass, subjected to thermal loading. To validate performance characteristics, a detailed finite element mathematical model is made, utilizing the NASTRAN digital routine. Included are typical Corning measured values of CTE, which vary positively and negatively within the mirror about a near zero nominal value. NASTRAN results under thermal soak and linear gradient conditions are compared to a theoretical solution of a partial shell under uniform axial thermal gradient.

Introduction

The manufacture of very large glass mirrors for ground based astronomical telescopes dictates scrutinous design analysis techniques. To this end, a study was undertaken to analytically investigate the optical performance in a thermal environment of such mirrors in light of boule variations in coefficient of thermal expansion. The imposed thermal environmental source was to consist of ambient soak variations as might occur on a daily basis, and axial gradient variations from solar irradiance.

Since the design of large mirrors tend toward manufacturing and weight limitations, a thin meniscus of glass was chosen for analysis. Chosen for investigation was a thin spherical mirror in the 50:1 diameter to thickness ratio region, a radical departure from conventional optics in the usual 6:1 regimes. For reasons of low coefficient of expansion to meet stringent optical performance requirements, typical properties of Corning Glass Works Ultra Low Expansion fused silica (ULE) glass were imposed, with negative and positive CTE values considered. Properties of ULE glass are such that detailed CTE axial and radial measurements throughout boule can be made. In this fashion, analytical correlation to typical real data could be obtained.

The body of this paper is concerned with the analytical approach utilized to determine the mirror errors resulting under an imposed thermal environment. Since a theoretical solution considering non-uniform CTE variations was unwieldy (if not impossible), the NASTRAN finite element digital computer routine was used. To accurately predict the thermal distortion, it was important to construct a model and compare results to a known theoretical solution. This accomplished, the model could be used to predict analytical results under a variety of conditions for mirrors of different sizes with a variable distribution of material CTE. Theoretical and finite element model results and comparisons are to be presented.

Math Model Description

Since the mirror facesheet exhibits quite variable albeit quite low coefficients of thermal expansion, it was necessary to map such values and variations one for one on our structural model to obtain an accurate solution under the thermal loading. This is done on the detailed NASTRAN model shown in Figure 1. The grid network consists of 979 node points, connected by 1056 finite elements. These are isoparametric bending-membrane elements. Element thermal strain data is mapped on each of these elements at five points through the thickness in order to properly account for the effective integrated strain gradient which could be non-linear. Thus, the model contains over 5000 temperature inputs for a given condition.

In order to obtain the analytical prediction of wavefront aberrations, representative manufacturer supplied coefficients of thermal expansion for typical boules comprising a facesheet were mapped onto the structural model. These are shown in Figure 2 at room temperature. This was accomplished via a specially written computer pre-processor which accounts for the profiles of the selective boules. The program then was utilized to map

the thermal profile from a thermal model and compute the effective thermal strain product ($\alpha\Delta T$) at each element at five points through its thickness. The output from this pre-processor was formulated to directly input to the NASTRAN model as a set of temperature cards. Finally, the deformed shapes obtained from the model were analyzed through the Itek optics post-processor routine to determine the components of the wavefront error (focus, astigmatism, coma, etc.).

Theoretical Analytical Solution

Because no closed form solution utilizing the variations of CTE and thermal non-uniformities could be obtained, the NASTRAN model was thoroughly scrutinized to ascertain its validity. The results of a uniform strain gradient were thus compared to a theoretical solution for both an assumed flat plate and actual spherical shell configuration.

It is easily shown that a kinematically mounted circular flat plate subjected to a linear thermal gradient through its thickness results in a spherical deformation well approximated by the relation:

$$y = \frac{\alpha\Delta T r^2}{2h} \tag{1}$$

where α is the material coefficient of thermal expansion, ΔT the difference in temperature between the top and bottom surfaces of the plate, r the plate radius and h the plate thickness.

For circular kenematic mirrors which have a finite radius of curvature, however, the mirror shell under the described gradient no longer remains in the stress free state afforded by the flat condition, so that equation (1) no longer applies. In this case, the thermal bending of a circular segment of a thin spherical shell subjected to a constant temperature gradient through its thickness is examined. The physical parameters are shown in Figure 3 and Table 1.

The deflections have been shown* to be equal to those at the same shell subjected to an edge moment, M, given by:

$$M = \frac{(\alpha\Delta T)D(1+\nu)}{h} \tag{2}$$

For uniform thickness shell segments of diameter less than one-half of the spherical radius (focal ratio, F>1, optically speaking) the shallow shell approximation** may be used. For the edge moment only case, the solution may be put in the form:

$$\frac{w}{\left(\frac{\alpha(\Delta T)r_1^2}{2h}\right)} = C_1[(\text{ber } x)-1] + C_2 \text{ bei } x \tag{3}$$

having chosen w=0 at x=r/ =0. Here $\frac{\alpha(\Delta T)r_1^2}{2h}$ is the (purely spherical) total deflection of a flat plate under the same strain gradient ($\alpha\Delta T/h$). C_1 and C_2 are given by (in matrix form)

$$\begin{array}{c|c|c} C_1 & & C_2 \\ \text{bei } x_1 + \frac{(1-\nu)\text{ber}'x_1}{x_1} & & -\left(\text{ber } x_1 - \frac{(1-\nu)\text{bei}'x_1}{x_1}\right) = \frac{2(1+\nu)}{x_1^2} \\ \hline \text{bei}'x_1 & & -\text{ber}'x_1 = 0 \end{array} \tag{4}$$

The determinant of the left matrix, Δ, is then

$$\Delta = -\text{ber}'x_1 \text{ bei } x_1 + \text{ber } x_1 \text{ bei}'x_1 - \frac{1-\nu}{x_1}\left[(\text{ber}'x_1)^2 + (\text{bei}'x_1)^2\right] \tag{5}$$

and the solution for C_1 and C_2 is

$$C_1 = \frac{2(1+\nu)}{x_1^2}\left(\text{ber}'x_1\right)\left(\frac{1}{\Delta}\right)$$

$$C_2 = \frac{2(1+\nu)}{x_1^2}\left(\text{bei}'x_1\right)\left(\frac{1}{\Delta}\right) \tag{6}$$

*Timoshenko, S. and S. Woinowsky - Krieger, "Theory of Plates and Shells", Second Edition McGraw-Hill, 1959, Article 129

**Ibid, Article 132

Infinite series for the Kelvin functions (ber, bei, etc. and combinations thereof), are found in Abramowitz and Stegun† (and no doubt in many other places). These may be used to express Δ, ber′, and bei′ as:

$$\Delta = \frac{(1+\nu)x_1}{4}\sum_{k=0}^{\infty}\left(\frac{x_1}{2}\right)^{4k}\frac{(2k+1+\nu)}{(1+\nu)(k!)^2((2k+1)!)(k+1)}$$

$$= \frac{(1+\nu)x_1}{4}\sum^{I} \tag{7}$$

$$\text{ber}'x_1 = -\frac{x_1^3}{2^3}\sum_{k=0}^{\infty}(-1)^k\left(\frac{x_1}{2}\right)^{4k}\frac{1}{(2k+2)!(2k+1)!}$$

$$= -\frac{x_1^3}{2^3}\sum^{II} \tag{8}$$

$$\text{bei}'x_1 = \frac{x_1}{2}\sum_{k=0}^{\infty}(-1)^k\left(\frac{x_1}{2}\right)^{4k}\frac{1}{(2k+1)!(2k)!}$$

$$= \frac{x_1}{2}\sum^{III} \tag{9}$$

† Abramowitz, A. and I.A. Stegun, "Handbook of Mathematical Functions", Dover, 1965.

us, defining $\sum^{I}$, $\sum^{II}$, $\sum^{III}$, C_1 and C_2 then become

$$C_1 = -\sum^{II}/\sum^{I}$$

$$C_2 = \frac{4}{x_1}\sum^{III}/\sum^{I} \tag{10}$$

expressing $r/r_1 = \rho = \frac{r}{\ell}\cdot\frac{\ell}{r_1}$, or $x = x_1\rho$

$$(\text{ber } x) - 1 = \sum_{k=1}^{\infty} \frac{(-1)^k \, x_1^{4k}\rho^{4k}}{2^{4k}\left((2k)!\right)^2} \tag{11}$$

(note summation starts at k=1)

$$\text{bei } x = \sum_{k=0}^{\infty} (-1)^k \left(\frac{x_1\rho}{2}\right)^{4k+2} \frac{1}{\left((2k+1)!\right)^2}$$

$$= \frac{x_1^2}{4} \sum_{k-0}^{\infty} (-1)^k \left(\frac{x_1}{2}\right)^{4k} \frac{\rho^{4k+2}}{\left((2k+1)!\right)^2} \tag{12}$$

we obtain $w/\frac{\alpha\Delta T r_1^2}{2h}$ as

$$w/\frac{\alpha\Delta T r_1^2}{2h} = \frac{\sum^{III}}{\sum^{I}} \sum_{k=0}^{\infty} (-1)^k \left(\frac{x_1}{2}\right)^{4k} \frac{\rho^{4k+2}}{\left((2k+1)!\right)^2}$$

$$+ \frac{\sum^{II}}{\sum^{I}} \sum_{k=1}^{\infty} (-1)^{k-1} \left(\frac{x_1}{2}\right)^{4k} \frac{\rho^{4k}}{\left((2k)!\right)^2} \tag{13}$$

It is this solution which must be compared to the finite element analysis. Since the output of that analysis is subject to optical post-processing to obtain rms deflection and aberation composition (particularly focus), it is convenient to express the power series above as a series in Zernike polynomials. These are orthogonal over the unit circle, $0 \leq \rho \leq 1$.

Restricting this attention of terms up to ρ^8, we can write

$$a_0 + a_2\rho^2 + a_4\rho^4 + a_6\rho^6 + a_8\rho^8$$

$$= b_0 Z_0 + b_2 Z_2 + b_4 Z_4 + b_6 Z_6 + b_8 Z_8 \tag{14}$$

in which $Z_0 = 1$

$Z_2 = 2\rho^2 - 1$

$Z_4 = 6\rho^4 - 6\rho^2 + 1$

$Z_6 = 20\rho^6 - 30\rho^4 + 12\rho^2 - 1$

$Z_8 = 70\rho^8 - 14\rho^6 + 90\rho^4 - 20\rho^2 + 1$

Equating coefficients of ρ^h provides a set of simultaneous equations from which the b_h can be solved. Expressing the normalization and orthogonality of the Zernike polynomials as

$$\int_0^1 Z_n Z_m \rho d\rho = \frac{1}{2(n+1)} \delta_{nm} \tag{15}$$

where δ_{nm} is the Kronecker delta (= 0 for $n \neq m$, = 1 for $n=m$), the rms deflection is found as

$$\sum_n \frac{\int_0^1 b_n^2 (Z_n)^2 \rho d\rho}{\int_0^1 \rho d\rho} = \sum_n \frac{b_n^2}{(n+1)}$$

$$\frac{w_{rms}}{\frac{\alpha \Delta Tr_1^2}{2h}} = \left(\frac{b_8^2}{9} + \frac{b_6^2}{7} + \frac{b_4^2}{5} + \frac{b_2^2}{3} \right)^{\frac{1}{2}} \tag{16}$$

or if the focal shift (ρ^2 term) is removed,

$$\frac{w_{rms}}{\frac{\alpha \Delta Tr_1^2}{2h}} = \left(\frac{b_8^2}{9} + \frac{b_6^2}{7} + \frac{b_4^2}{5} \right)^{\frac{1}{2}} \tag{17}$$

These values are now compared with the finite element calculations to follow below.

Finite Element and Theoretical Comparisons

To illustrate what happens to the residual error before and after focus correction, the detailed NASTRAN model of 40 inch diameter mirror was made, with the mirror thickness varied accordingly. The model was initially run as a flat plate, and the results found to agree with the theoretical solution to within one-half of a percent. A radius of curvature of 175 inches was then included to represent a typical curved optic.

Utilizing a constant unit gradient through the mirror thickness, the resulting displacements from the math model were then input to the Itek OPTICS Package to determine residual error both before and after focus. The results are shown in Figure 4, along side the theoretical solution afforded in the paragraphs above. The correlation is markedly good.

As evidenced by the curves, the departure from the flat plate error is most pronounced as the diameter to thickness ratio increases. For a D/t of 50:1, as is our design, the error is about 2.5 times less than the flat plate without correction. After focus, however, about 16 percent residual still remains, whereas the flat plate error is entirely focusable. For a D/t of 10:1, the uncorrected error is very close to that of the flat plate, while the residual error remaining after focus is less than 1 percent.

We conclude that the shell effect reduces the residual error before a focus fit, under a thermal axial gradient. After focus, the residual error may be significant. This phenomenon, again, is validated by the shell theory earlier presented.

Thermal Performance Under Various Thermal Levels

Satisfied with the model performance, various thermal levels were superimposed, as could occur under solar load.

Soak and gradient values were incorporated to the NASTRAN model in conjunction with the measured CTE data across the facesheet as illustrated in Figure 2. The Corning measured values, however, are valid only near room temperature. As temperature increases,

the thermal strain behavior of ULE glass is non-linear; that is, the coefficient of thermal expansion is not a constant. This is evident by the thermal expansion strain curves for ULE glass shown in Figure 5. Thus, the facesheet room temperature data were imposed upon these curves to obtain the true variation of strain over the entire region of the flux level loading. For ease in programming to the preprocessor which would generate the temperature cards necessary for the NASTRAN program, a table look up interpolation chart was prepared to generate an effective coefficient of thermal expansion at any temperature input as predicted by the thermal analysis. The effective coefficient of expansion is defined as the total strain to the temperature level of interest divided by the temperature change. It is noted that at higher temperature levels, effective CTE is increased markedly from the room temperature level, as enhanced in Table 2. These must be duly considered to obtain meaningful results.

Analytical Results

Responding to a potential need for large but light ground based astronomical telescopes, the NASTRAN mathematical model was scaled to yield a 300 inch diameter by 5 inch thick F/2 curved optic which might be subject to daily thermal variations. As before, coefficient of thermal expansion was varied throughout the model, representative of typical ULE data. Variations of $\pm.015 \times 10^{-6}/°C$ about a nominal value were thus considered, after initially imposing a uniform CTE field. The mirror was independently subjected to a 1°C soak and 1°C axial gradient, and the results post-processed to obtain the rms error before and after focus correction.

The results for these cases are shown in Table 3. For the case of a uniform soak and uniform CTE, the residual error is small before focus and entirely correctable after focus. When the radial variations of CTE are considered, the uniform soak case yields a tenfold greater error before focus, less than fifty percent of which is refocusable.

For the case of a uniform axial gradient, it is noted that nearly thirty percent residual error remains after focus, with no variation in CTE. This is in agreement with the theoretical results earlier presented. Imposition of variation of CTE for the gradient case further increases the error residual. While errors are small, larger soaks and gradients could demand other compensation techniques.

Conclusion

Based on the results above, it is concluded that the NASTRAN finite element analysis affords an excellent correlation to the shell theory, utilizing isoparametric bending-membrane elements in sufficient detail. Credibility is thus afforded when variations in coefficient of thermal expansion are considered. Provided that thermal strain variation with temperature is duly considered, optical aberrations are able to be extrapolated to various levels of thermal exposure. Finally, it is concluded that for large thin optics, uniformity in thermal environment does not preclude residual error after focus, so that other compensation techniques may need be considered.

Acknowledgements

The authors wish to thank the multitude of talented individuals of Itek Optical Systems, Lexington, MA who were involved with analysis and modeling of the subject mirrors. Special thanks are gratefully afforded to Mrs. Cherie Draskovich, for her care and efforts in typing the manuscript.

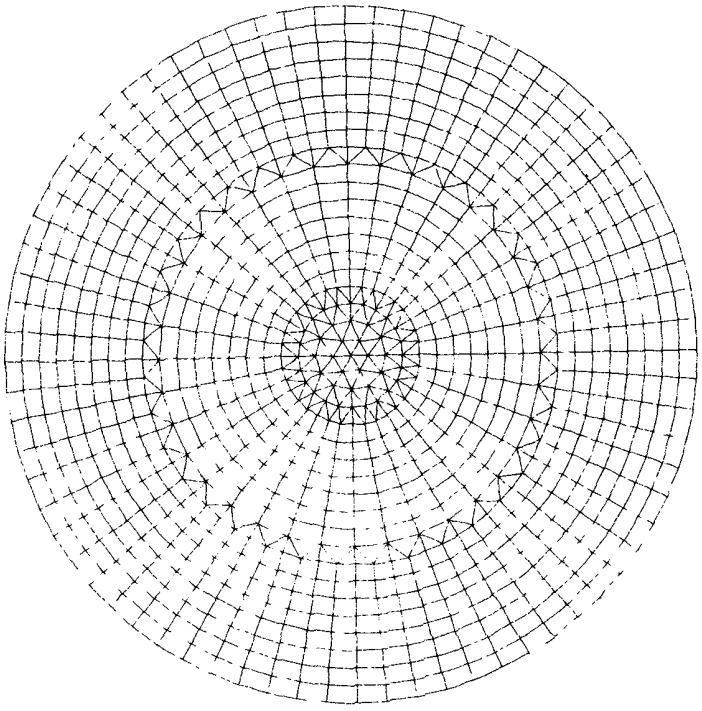

(Plan View)

Fig. 1. NASTRAN structural model

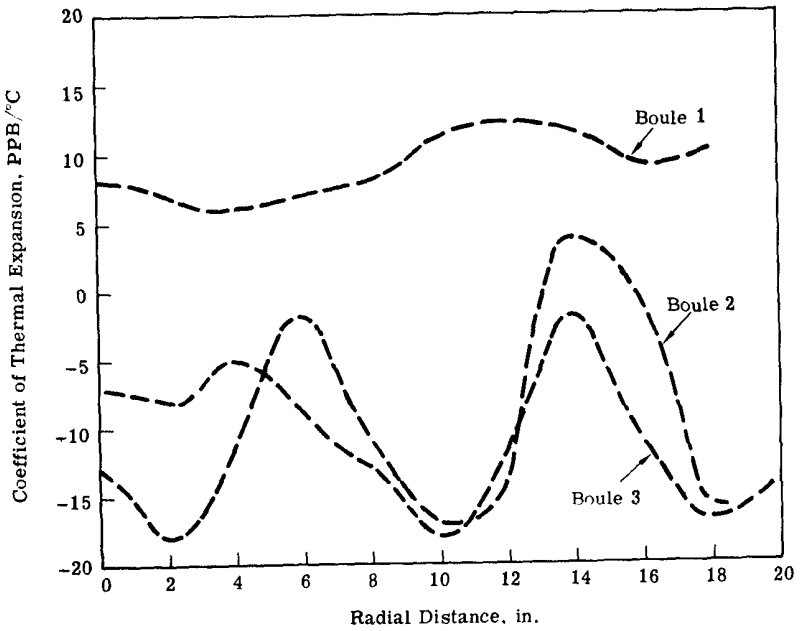

Fig. 2. Typical CTE variations in ULE boules

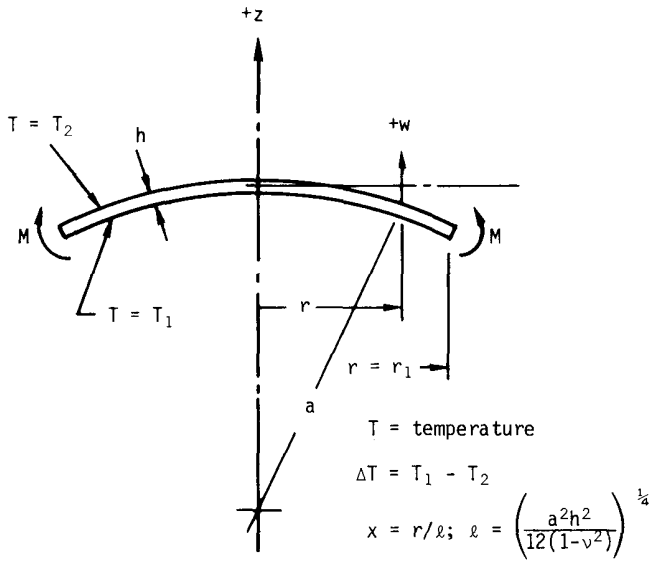

Fig. 3. Spherical shell parameters

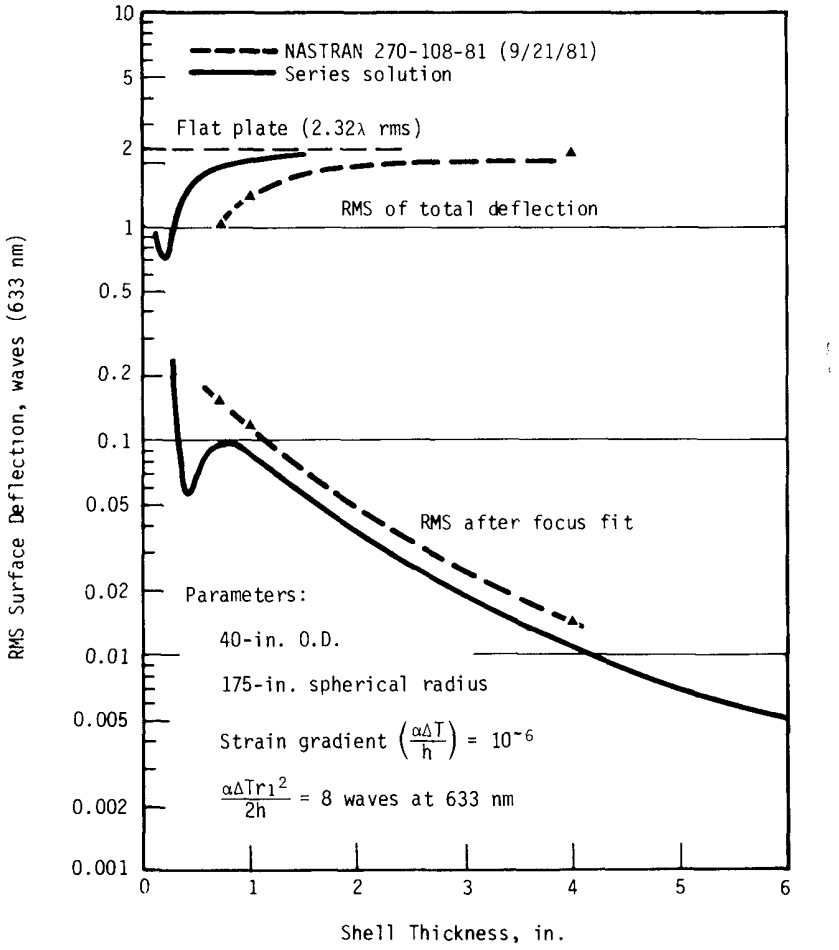

Fig. 4. Comparison of series solution with finite element solution

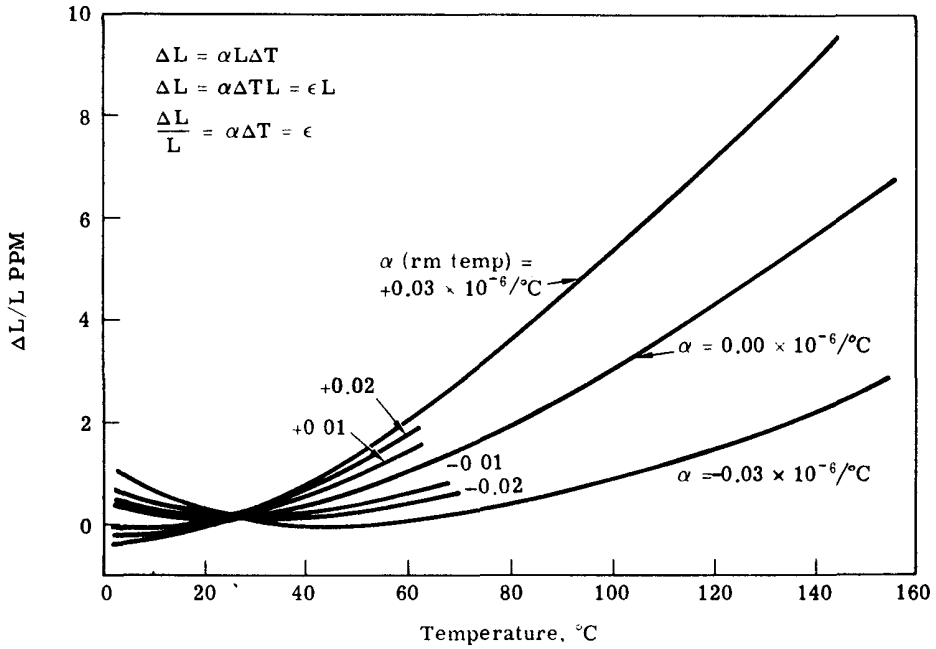

Fig. 5. Thermal expansion for code 7971 ULE (Corning G. W. measured data)

Table 1. Nomenclature

M	=	edge moment equivalent for thermal bending
α	=	thermal expansion coefficient
ΔT	=	T_1-T_2 = temperature difference across shell
D	=	$Eh^3/12(1-\nu^2)$ for the shell
E	=	Young's modulus for the shell material
h	=	shell thickness
ν	=	Poisson's ratio for the shell material
r	=	distance from axis of revolution of the circular shell segment
r_1	=	r at outer edge
x	=	r/ℓ
ℓ	=	$\left(a^2h^2/12(1-\nu^2)\right)^{\frac{1}{4}}$
a	=	shell spherical radius
ber,bei	=	Kelvin (Thomson) functions, which are Bessel functions with complex argument
′	=	denotes differentation with respect to the argument of a function
w	=	shell deflection in the axial (+Z) direction

Table 2. Coefficient of Thermal Expansion

($68^{\circ}F$) $20^{\circ}C$ (Measured values)	($104^{\circ}F$) $20\text{-}40^{\circ}C$	($140^{\circ}F$) $20\text{-}60^{\circ}C$	Difference (max-RT)
$-.018 \times 10^{-6}$	$-.010 \times 10^{-6}$	$+.007 \times 10^{-6}$	$.025 \times 10^{-6}$/
-.017	-.008	+.008	.025
-.016	-.004	+.009	.025
-.014	+.000	+.010	.024
-.013	+.005	+.013	.026
-.011	+.010	+.018	.029
-.009	+.010	+.019	.028
-.008	+.011	+.020	.028
-.007	+.012	+.021	.028
-.005	+.012	+.022	.027
-.002	+.014	+.025	.027
-.001	+.015	+.028	.029
+.004	+.017	+.029	.025
+.006	+.018	+.030	.024
+.007	+.020	+.031	.024
+.008	+.022	+.032	.024
+.009	+.024	+.034	.025
+.010	+.025	+.035	.025
+.011	+.026	+.038	.027
+.012	+.027	+.040	.028

Table 3. Response to Soak and Gradient for a 300 x 5-In.-Thick ULE Curved Optic

	1°C Soak Change		1°C Axial Gradient	
	Error From Perfect CTE Value	Error From Radial CTE Variation	Error From Perfect CTE Value	Error From Radial CTE Variation
Uncorrected	0.0024	0.032	0.131	0.073
Focus	0.0000	0.019	0.037	0.046

- All values in waves (surface) at 633 nm
- Nominal perfect CTE $0.015 \times 10^{-6}/°C$
- Radial CTE variation $\pm 0.015 \times 10^{-6}/°C$